MINUSTRY OF EDUCATION AND TRAINING
HANOI PEDAGOGICAL UNIVERSITY 2
—————o0o—————

PHAM DUY THANH

THEORETICAL STUDY ON THERMODYNAMIC PROPERTIES OF DILUTE BOSE GASES AT ULTRA-LOW TEMPERATURES

Major: **Theoretical Physics and Mathematical Physics**

Code: **9 44 01 03**

SUMMARY OF THE DOCTORAL THESIS IN PHYSICS

Supervisor: **Assoc. Prof. Dr. NGUYEN VAN THU**

HANOI, 2026

The doctoral thesis was completed at
Hanoi Pedagogical University 2

Supervisor: Assoc. Prof. Dr. Nguyen Van Thu

Reviewer:

Reviewer:

Reviewer:

The doctoral thesis will be defended before the University Thesis Examining Council at Hanoi Pedagogical University 2 at

The doctoral thesis can be found at:

- National Library of Vietnam
- Library of Hanoi Pedagogical University 2

Introduction

1 Reason for choosing the topic

The phenomenon of Bose–Einstein condensation, theoretically predicted by Einstein in 1924, is one of the most remarkable phenomena in quantum field theory, statistical physics, and the study of many-body systems. Although the Gross–Pitaevskii (GP) theory describes the dilute Bose gas quite well at zero temperature, it remains limited when addressing systems at finite temperature. The effective action Cornwall–Jackiw–Tomboulis (CJT) formalism provides a consistent theoretical framework that allows the study of both equilibrium thermodynamics and nonequilibrium dynamics of many-body systems. Within this context, research on phase transitions and surface effects of Bose systems has become increasingly attractive in modern theoretical physics.

For these reasons, we have chosen the topic: "Theoretical study on thermodynamic properties of dilute Bose gases at ultra-low temperatures". In particular, this thesis focuses on determining static quantities of the prewetting phase in the binary mixtures of Bose–Einstein condensate (BEC) within the GP framework and analyzing the thermodynamic behavior of the interacting Bose gas at finite temperatures within the CJT formalism.

2 The aims of thesis

This thesis aims to achieve two main objectives:

1. To determine the characteristics of the prewetting transition in binary mixtures of BEC. The expected results may contribute to the understanding and potential design of systems exhibiting Bose–Einstein condensation in confined geometries.

2. To determine BEC critical temperature and the thermodynamic quantities of the dilute Bose gas at finite temperatures. On this basis, the study aims to provide insight into the thermal behavior of the system beyond the mean-field approximation.

3 The object and scope of thesis

The object of study of this dissertation is a weakly interacting, dilute Bose gas, consisting of one or two components, at temperatures extremely low compared to room temperature (on the order of several tens to several hundreds of nanokelvin), covering both the temperature regimes above and below the Bose–Einstein condensation transition temperature.

The scope of the study includes:

For the two-component Bose gas: the doctoral thesis investigates the system in an inhomogeneous spatial domain at zero temperature.

For the single-component Bose gas: the doctoral thesis considers a homogeneous dilute Bose gas at finite temperature, specifically focusing on the BEC critical transition temperature T_c and on the regime of temperatures much lower than T_c (which is called the near-zero temperature region in the thesis).

4 Research tasks

In this thesis, we focus on the following research problems:

1. The prewetting phase in binary mixtures of BEC.

2. The theory of BEC at finite temperature near the boundary within the Hartree–Fock–Bogoliubov (HFB) framework.

3. The thermodynamic properties of the dilute Bose gas in condensed phase at ultra–low temperatures.

4. The BEC critical temperature of a dilute weakly interacting Bose gas.

5.The thermodynamic properties of a dilute Bose gas near the critical point of condensed phase transition.

5 Research methods

In this thesis, we employ the following theoretical methods:

1. For the study of the dilute Bose gas at zero temperature, we use the Gross–Pitaevskii (GP) theory. Since the GP equation does not have an exact analytical solution for the system's order parameter in the presence of external potentials, we adopt an approximate solution using the double-parabola approximation (DPA). The effects of boundary potentials and geometric confinement are analyzed and incorporated within this approach.

2. For the study of the dilute Bose gas at finite temperatures, we employ the CJT formalism, where the effective action is constructed as a functional of both the mean field and the propagator. Because determining the exact form of the effective action is generally intractable, we use the Hartree–Fock approximation as a self-consistent and practical approach. The effects of external potentials and temperature are analyzed within this theoretical framework.

6 The contributions of the thesis

The thesis contributes new results concerning the thermodynamic properties of the dilute Bose gas at ultra-low temperatures. The main scientific contributions are presented in detail in the Conclusion section of the thesis.

7 The structure of the thesis

Apart from the Introduction, Conclusion, References, and Appendices, the main content of the dissertation is organized into four chapters:

Chapter 1: Overview of Bose–Einstein condensation.

Chapter 2: Approximate methods.

Chapter 3: Thermodynamic properties of dilute Bose gas at zero temperature.

Chapter 4: Thermodynamic properties of dilute Bose gas at finite temperature.

Chapter 1

Overview of Bose–Einstein condensation

1.1 Bose–Einstein condensation

1.1.1 Bose–Einstein statistics

According to quantum statistical mechanics, the average number of bosons occupying a single-particle state $|n_i\rangle$ with energy level ε_i is given by

$$\langle n_i \rangle = \frac{1}{e^{\beta(\varepsilon_i - \mu)} - 1}, \tag{1.1}$$

where $\beta = (k_{\mathrm{B}}T)^{-1}$ with T being the temperature and k_{B} is the Boltzmann constant. The right-hand side of the above equation is known as the *Bose–Einstein distribution function*.

1.1.2 The condensation of Bose gas

The average number of particles in the ground state ($\varepsilon_0 = 0$) is

$$\langle n_0 \rangle = \frac{1}{e^{-\beta\mu} - 1}, \tag{1.2}$$

and therefore, a macroscopic number of particles will accumulate in the ground state when the chemical potential μ approaches zero from below.

The critical temperature of an ideal Bose gas is determined as

$$T_{\mathrm{c}} = \frac{2\pi\hbar^2}{m k_{\mathrm{B}}} \left(\frac{\rho}{\zeta(3/2)} \right)^{2/3} \approx 3.31 \frac{\hbar^2 \rho^{2/3}}{m k_{\mathrm{B}}}, \tag{1.3}$$

where $\rho = N/V$ is the particle density.

The number of condensed particles N_0 in the ideal Bose gas at temperature T ($< T_{\mathrm{c}}$) is given by

$$N_0 = N - N_{\mathrm{ex}} = N \left[1 - \left(\frac{T}{T_{\mathrm{c}}} \right)^{3/2} \right]. \tag{1.4}$$

According to the Bogoliubov theory of weakly interacting Bose gases and the Lee–Huang–Yang correction, the depletion fraction of the condensate at zero temperature is

$$\frac{N_{\mathrm{ex}}}{N} = \frac{8}{3\sqrt{\pi}} \sqrt{\rho a_s^3}, \tag{1.5}$$

where a_s is the *s-wave scattering length*.

1.2 Experimental results on Bose–Einstein condensation

1.2.1 Experimental observation of Bose gas condensation

In June 1995, Cornell and Wieman at JILA (Joint Institute for Laboratory Astrophysics) first observed the Bose–Einstein condensation when cooling a dilute gas of Rubidium-87 (^{87}Rb) atoms down to 170 nK creating a condensate state of about 2000 atoms. The formation of the BEC was confirmed by the appearance of a sharp peak in the velocity distribution, which was measured using the time-of-flight (TOF) imaging technique. Shortly thereafter, Ketterle at the Massachusetts Institute of Technology (MIT) (September 1995) created a BEC of Sodium-23 (^{23}Na) atoms at 200 nK. These pioneering experiments marked a breakthrough and spurred rapid developments in both experimental and theoretical studies of BEC.

1.2.2 Experimental observation of Bose mixture condensation

After the first realization of Bose–Einstein condensation, subsequent experiments were extended to study multi-component BEC mixtures, consisting of different atomic species or different hyperfine states of the same atom. The development of cooling and trapping techniques, as well as the control of interatomic interactions through Feshbach resonances, has allowed for the observation of many remarkable phenomena, including phase separation and miscibility transitions between condensate components. These experimental findings have provided valuable insights into both the static and dynamic properties of ultracold Bose systems, thereby establishing an important foundation for the study of quantum many-body systems.

1.2.3 Hard-wall confinement technology

Two main techniques have been developed to create hard-wall potentials (or box traps) for BECs: one based on evanescent wave reflection from a dielectric surface, and the other using optical or magnetic mirror configurations. These methods allow researchers to confine the condensate in nearly uniform density conditions, providing an ideal platform to study thermodynamic quantities and quantum correlations in homogeneous Bose gases.

1.3 Theoretical approaches to Bose–Einstein condensation

1.3.1 Gross–Pitaevskii theory

The time-dependent Gross–Pitaevskii (GP) equation that describes the condensate wave function is given by

$$i\hbar\frac{\partial\Psi(\mathbf{r},t)}{\partial t} = \left(-\frac{\hbar^2}{2m}\nabla^2 + V_{\text{ext}}(\mathbf{r}) + g|\Psi(\mathbf{r},t)|^2\right)\Psi(\mathbf{r},t), \tag{1.6}$$

where $g = \dfrac{4\pi\hbar^2}{m}a_s$ is the coupling constant and a_s is the s-wave scattering length.

In the ground state, the condensate wave function can be written as

$$\Psi(\mathbf{r},t) = \Psi_0(\mathbf{r})e^{-i\frac{\mu t}{\hbar}}, \tag{1.7}$$

where μ is the chemical potential and Ψ_0 is a real function satisfying the normalization condition $\int d\mathbf{r}\Psi_0^2 = N_0 = N$. Substituting Eq. (1.7) into Eq. (1.6), we obtain the time-independent Gross–Pitaevskii equation (TIGP):

$$\left(-\frac{\hbar^2}{2m}\nabla^2 + V_{\text{ext}}(\mathbf{r}) + g\Psi_0^2(\mathbf{r})\right)\Psi_0(\mathbf{r}) = \mu\Psi_0(\mathbf{r}). \tag{1.8}$$

1.3.2 Cornwall–Jackiw–Tomboulis effective action approach

In the absence of external sources ($J = K = 0$), the stationary state of the system satisfies

$$\frac{\delta\Gamma[\Psi_0, G]}{\delta\Psi_0} = 0, \tag{1.9}$$

and the Schwinger–Dyson (SD) equation

$$\frac{\delta\Gamma[\Psi_0, G]}{\delta G} = 0, \tag{1.10}$$

where $\Gamma[\Psi_0, G]$ is the two-particle irreducible (2PI) effective action defined as:

$$\Gamma[\Psi_0, G] = S_0[\Psi_0] + \frac{i\hbar}{2}\,\mathrm{tr}\left(\ln G^{-1} + G_0^{-1}(\Psi_0)G - \mathbb{1}\right) + \Gamma_2[\Psi_0, G]. \tag{1.11}$$

The thermodynamic potential in the CJT formalism is then expressed as:

$$V_{\text{CJT}} = V_0(\Psi_0) - \frac{i\hbar}{2}\int\frac{d^4k}{(2\pi)^4}\,\mathrm{tr}\left[\ln G^{-1}(k) + G_0^{-1}(k)G(k) - \mathbb{1}\right] + V_2[\Psi_0, G], \tag{1.12}$$

where $V_0(\Psi_0)$ is the classical potential.

Chapter 2

Approximate methods

2.1 Doule-parabola approximation

2.1.1 Double-parabola approximation for one-component BEC

The basic idea of DPA is to replace the quartic Gross–Pitaevskii (GP) potential

$$V_{\mathrm{GP}} = -\mu|\Psi_0|^2 + \frac{g}{2}|\Psi_0|^4 \tag{2.1}$$

with a quadratic potential (referred to as the DPA potential)

$$V_{\mathrm{DPA}}(\Psi_0) = g\rho^2\left[2\left(1-\frac{\sqrt{|\Psi_0|^2}}{\sqrt{\rho}}\right)^2 - \frac{1}{2}\right]. \tag{2.2}$$

This substitution turns the GP equation describing the condensate wave function into a linear differential equation, from which we can easily find its analytical solution.

2.1.2 Double-parabola approximation for two-component BEC

The dimensionless TIGP equations describing the dimensionless condensate wave functions of the system take the form:

$$\begin{aligned} -\frac{d^2\psi_1}{d\tilde{z}^2} - \psi_1 + \psi_1^3 + K|\psi_2|^2\psi_1 = 0, \\ -\xi^2\frac{d^2\psi_2}{d\tilde{z}^2} - \psi_2 + \psi_2^3 + K|\psi_1|^2\psi_2 = 0. \end{aligned} \tag{2.3}$$

Considering the case where the two condensate components coexist in equilibrium in the bulk phase and in an infinitely extended space, we have the following Dirichlet boundary conditions:

$$\begin{aligned} \psi_1(-\infty) = \psi_2(\infty) = 0, \\ \psi_2(-\infty) = \psi_1(\infty) = 1. \end{aligned} \tag{2.4}$$

To obtain the analytical expression of ψ_j for arbitrary values of K and ξ, the DPA method must be employed, in which the dimensionless GP potential of the two-component BEC system is replaced by the dimensionless DPA potential:

$$\mathcal{V}_{\mathrm{DPA}}(\psi_1,\psi_2) = 2(|\psi_j|-1)^2 + (K-1)|\psi_{j'}|^2 - \frac{1}{2}, \tag{2.5}$$

The result is the emergence of two independent linear equations that approximately describe the reduced order parameters of the system:

$$\begin{aligned} -\frac{d^2\psi_j}{d\tilde{z}^2} + 2(\psi_j - 1) = 0, \\ -\xi^2\frac{d^2\psi_{j'}}{d\tilde{z}^2} + (K-1)\psi_{j'} = 0. \end{aligned} \tag{2.6}$$

The corresponding solutions of the two equations above are

$$\begin{aligned} \psi_j(\tilde{z}) &= 1 - \frac{\sqrt{K+1}}{\sqrt{2}+\sqrt{K+1}} \exp\left(-\sqrt{2}|\tilde{z}|\right), \\ \psi_{j'}(\tilde{z}) &= \frac{\sqrt{K-1}}{\sqrt{2}+\sqrt{K-1}} \exp\left(-\frac{\sqrt{K-1}}{\xi}|\tilde{z}|\right), \end{aligned} \tag{2.7}$$

with $(j, j') = (1, 2)$ if $z \geq 0$ and $(j, j') = (2, 1)$ if $z \leq 0$.

2.2 Hartree–Fock approximation

In the Hartree–Fock approximation (HFA), we retain only the simplest 2PI contribution in the functional Γ_2 of the CJT effective action, namely the double-bubble diagram. This diagram consistently represents the lowest-order self-interaction effects in a nonperturbative manner, while simultaneously performing an infinite summation over a class of perturbative diagrams, specifically, the so-called "daisy" and "superdaisy" diagrams. In addition, it accounts for mean-field effects such as direct (Hartree) interactions and, in certain systems, also exchange (Fock) interactions.

2.2.1 The interaction Lagrangian density in HFA

In the Ψ^4 theory, the Lagrangian density is

$$\mathcal{L}[\Psi, \Psi^*] = \Psi^* \left(-i\hbar\frac{\partial}{\partial t} - \frac{\hbar^2}{2m}\nabla^2\right)\Psi - \mu|\Psi|^2 + \frac{g}{2}|\Psi|^4. \tag{2.8}$$

Within the imaginary-time formalism at finite temperature T, the CJT effective potential density takes the form:

$$V_{\text{CJT}} = -\mu\Psi_0^2 + \frac{1}{2}\int_\beta \text{tr}\left[\ln G^{-1}(k) + G_0^{-1}(k)G(k) - \mathbb{1}\right] + V_2(\Psi_0, G), \tag{2.9}$$

In the above equation, the symbol $\int_\beta$ is defined as:

$$\int_\beta f(k) \equiv \frac{1}{\beta}\sum_{n=-\infty}^{+\infty}\int\frac{d^3\mathbf{k}}{(2\pi)^3} f(\omega_n, |\mathbf{k}—). \tag{2.10}$$

with $\omega_n = 2n\pi\hbar^{-1}\beta^{-1}$ are the bosonic Matsubara frequencies.

The expression of $V_2(\Psi_0, G)$ in HFA is given by:

$$V_2(\Psi_0, G) = \frac{g}{2}\Psi_0^4 + \frac{g}{2}\Psi_0^2(3P_{11} + P_{22}) + \frac{g}{4}P_{11}P_{22} + \frac{3g}{8}\left(P_{11}^2 + P_{22}^2\right), \tag{2.11}$$

where $P_{jj} = \int_\beta G_{jj}(k)$ (with $j = 1, 2$) are the loops representing the momentum integrals in momentum space.

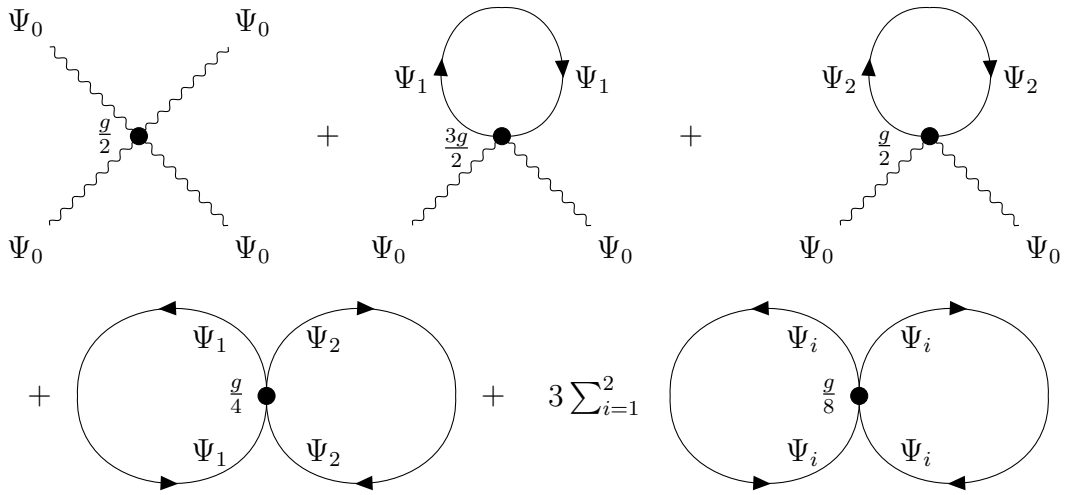

Figure 2.1: Feynman 2PI diagrams corresponding to LW functional.

2.2.2 Tree-level approximation

In the tree-level approximation, the effective potential density takes the form:

$$V_{\mathrm{CJT}} = -\mu\Psi_0^2 + \frac{g}{2}\Psi_0^4. \tag{2.12}$$

2.2.3 One-loop approximation

In the one-loop approximation, the effective potential density takes the form:

$$V_{\mathrm{CJT}} = -\mu\Psi_0^2 + \frac{g}{2}\Psi_0^4 + \frac{1}{2}\int_\beta \mathrm{tr}\left[\ln G^{-1}(k)\right]. \tag{2.13}$$

2.2.4 Two-loop approximation

In the two-loop approximation, the effective potential density takes the form:

$$\begin{aligned} V_{\mathrm{CJT}} = &-\mu\Psi_0^2 + \frac{g}{2}\Psi_0^4 + \frac{1}{2}\int_\beta \mathrm{tr}\left[\ln G^{-1}(k) + G_0^{-1}(k)G(k) - \mathbb{1}\right] \\ &+ \frac{3g}{8}\left(P_{11}^2 + P_{22}^2\right) + \frac{g}{4}P_{11}P_{22}. \end{aligned} \tag{2.14}$$

Chapter 3

Thermodynamic properties of dilute Bose gas at zero temperature

3.1 Ground state of a two-component BEC in a semi-infinite space

We consider a two-component BEC system that is translationally symmetric in the (x, y) plane and confined by a hard-wall located at $z = 0$. On the other side, instead of keeping the particle number fixed, we consider the system at fixed chemical potentials. We assume that the component 1 is in a stable bulk phase with chemical potential $\mu_1 = \bar{\mu}_1$ and density $\rho_1 = \mu_1/g_{11}$. Meanwhile, the condensate 2 with chemical potential μ_2 and density ρ_2 has not yet reached bulk phase equilibrium. The bulk two-phase coexistence of the system is achieved if the chemical potential and density of condensate 2 are respectively given by $\mu_2 = \bar{\mu}_2 = \mu_1\sqrt{g_{22}/g_{11}}$ và $\rho_2 = \bar{\rho}_2 = \bar{\mu}_2/g_{22}$.

The dimensionless TIGP equations describing the reduced order parameters of the system are written as:

$$-\frac{d^2\psi_1}{d\tilde{z}^2} - \psi_1 + \psi_1^3 + K\psi_2^2\psi_1 = 0, \tag{3.1a}$$

$$-\xi^2\frac{d^2\psi_2}{d\tilde{z}^2} - \epsilon\psi_2 + \psi_2^3 + K\psi_1^2\psi_2 = 0, \tag{3.1b}$$

with the corresponding boundary conditions: $\psi_1(0) = \psi_2(0) = \psi_2(\infty) = 0,\ \psi_1(\infty) = 1$.

The quantity ϵ on the left-hand side of Eq. (3.1b) is defined as $\epsilon = \mu_2/\bar{\mu}_2$ and is referred to as the chemical potential ratio. By applying DPA model, we obtain the reduced order parameters of the system as follows:

- In the region to the right of the interface ($\tilde{z} > 0$):

$$\psi_1(\tilde{z}) = 1 + A_1 e^{-\sqrt{2}\tilde{z}} \tag{3.2a}$$

$$\psi_2(\tilde{z}) = B_1 \exp\left(-\frac{\sqrt{K-\epsilon}}{\xi}\tilde{z}\right). \tag{3.2b}$$

- In the region to the left of the interface ($\tilde{z} < 0$):

$$\psi_1(\tilde{z}) = 2A_2 \sinh\left(\sqrt{\epsilon K - 1}\tilde{z}\right), \tag{3.3a}$$

$$\psi_2(\tilde{z}) = 2B_2 \sinh\left(\frac{\sqrt{2\epsilon}}{\xi}\tilde{z}\right) + \sqrt{\epsilon}\left[1 - \exp\left(-\frac{\sqrt{2\epsilon}}{\xi}\tilde{z}\right)\right]. \tag{3.3b}$$

The coefficients A_1, A_2, B_1 and B_2 are determined from the continuous conditions of the reduced order parameters and their first derivatives at the interface position ($\tilde{z} = \tilde{\ell}$).

3.2 Wetting phase diagram

We consider the nucleation process, in which component 2 begins to form within component 1. In this case, ψ_2 is small compared to unity, and the system of equations becomes

$$-\frac{d^2\psi_1}{d\tilde{z}^2} - \psi_1 + \psi_1^3 = 0, \tag{3.4a}$$

$$-\xi^2\frac{d^2\psi_2}{d\tilde{z}^2} - \epsilon\psi_2 + K\psi_1^2\psi_2 = 0, \tag{3.4b}$$

Solving the above system of eigenfunction-eigenvalue equations yields

$$\epsilon_n = K - \frac{\xi^2}{2}\left[\frac{1}{2}\sqrt{1+\frac{8K}{\xi^2}} - \left(n+\frac{1}{2}\right)\right]^2, \ n = 1, 2, 3, ... \tag{3.5}$$

$$\psi_2(\tilde{z}) = \left[\cosh\left(\frac{\tilde{z}}{\sqrt{2}}\right)\right]^{-\sqrt{2}\xi_1/\Lambda_2}\sum_{m=0}^{n} c_m\left[\tanh\left(\frac{\tilde{z}}{\sqrt{2}}\right)\right]^m. \tag{3.6}$$

The boundary condition $\psi_2(0) = a_0 = 0$ leads to $a_2 = 0$. From this, it follows that the unique eigenvalue corresponding to $n = 1$ is

$$\epsilon = K - \frac{\xi^2}{8}\left[\sqrt{1+\frac{8K}{\xi^2}} - 3\right]^2. \tag{3.7}$$

To verify the analytical results obtained, we plot the order parameter profiles as shown in Fig. 3.1. The good agreement between the plots confirms the accuracy of our analytical solution.

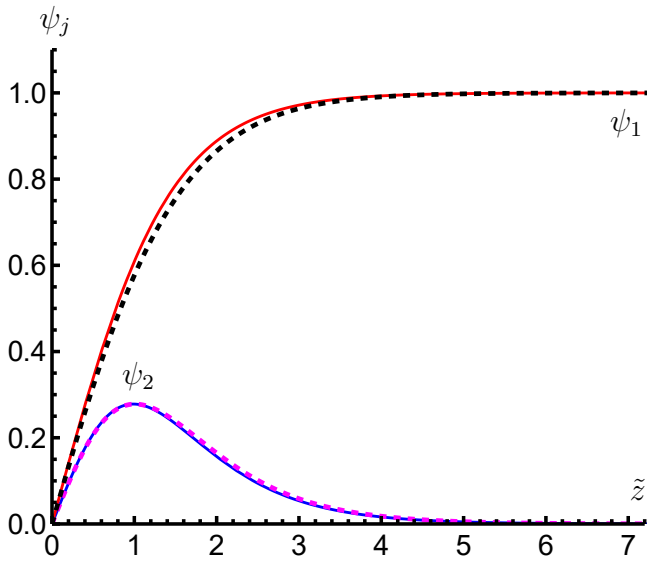

Figure 3.1: The plot shows the reduced order parameters as functions of $\tilde{z}$ for $\epsilon = 0.92$, $\xi = 1/2$, and $K = 1.3$. The solid lines represent the analytical results, while the dashed lines represent the numerical results.

In Fig. 3.2, the immiscible region is separated from the miscible region by the line segment MN, which corresponds to the demixing states with $K = 1$.

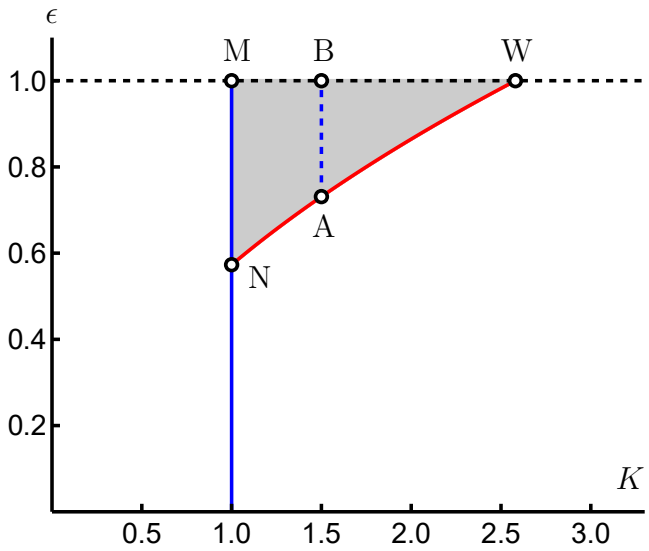

Figure 3.2: The nucleation line for $\xi = 1/3$. The gray region shown in the plot represents the prewetting region.

We consider the case corresponding to Fig. 3.2 where the relative healing length is $\xi = 1/3$. The non-wetting domain of the interface is represented by the gray area. At the wetting point W, the chemical potential ratio ϵ corresponding to the bulk two-phase coexistence. At this point, the auxiliary healing length of condensate 2, $\bar{\xi}_2$, satisfies the condition $\bar{\xi}_2 = \xi_2$ (or $\epsilon = 1$). The nucleation line intersects the coexistence line at point W, and the corresponding relative interaction strength K is denoted by K_{wet}. From (3.7), we obtain the following relation:

$$K_{\text{wet}} = \epsilon + \frac{2}{9}\left(\frac{\epsilon}{\xi} - \xi\right)^2. \tag{3.8}$$

It is easy to see that the maximum value of K_{wet} increases as ξ decreases. For $\xi = 1/3$, we have $K_{\text{wet}} \leq 2.58$, and this range of K is suitable for experimental tunability.

We assume that $\xi_2 < \xi_1$. Therefore, the wetting transition cannot occur when the wall tension γ_{W_1} of component 1 is smaller than the sum of the wall tension γ_{W_2} of component 2 and the interfacial tension γ_{12}. This condition is expressed by the inequality:

$$\gamma_{\text{W1}} < \gamma_{\text{W2}} + \gamma_{12}. \tag{3.9}$$

The above condition is equivalent to

$$K > \epsilon + \frac{2}{9}\left(\frac{\epsilon}{\xi} - \xi\right)^2 = K_{\text{wet}}. \tag{3.10}$$

This inequality defines the range of the relative interaction strength K in which the wetting transition cannot occur. In other words, the prewetting stage takes place in the range $1 < K \leq K_{\text{wet}}$. In the wetting phase diagram (Fig. 3.2), the prewetting state corresponds to the MNW region (the gray area). The wetting transition occurs when $1 < K \leq K_{\text{wet}}$ and $\epsilon = 1$. Below the red segment NW, nucleation does not take place.

3.3 Static properties of prewetting phase

3.3.1 Thickness of the prewetting layer

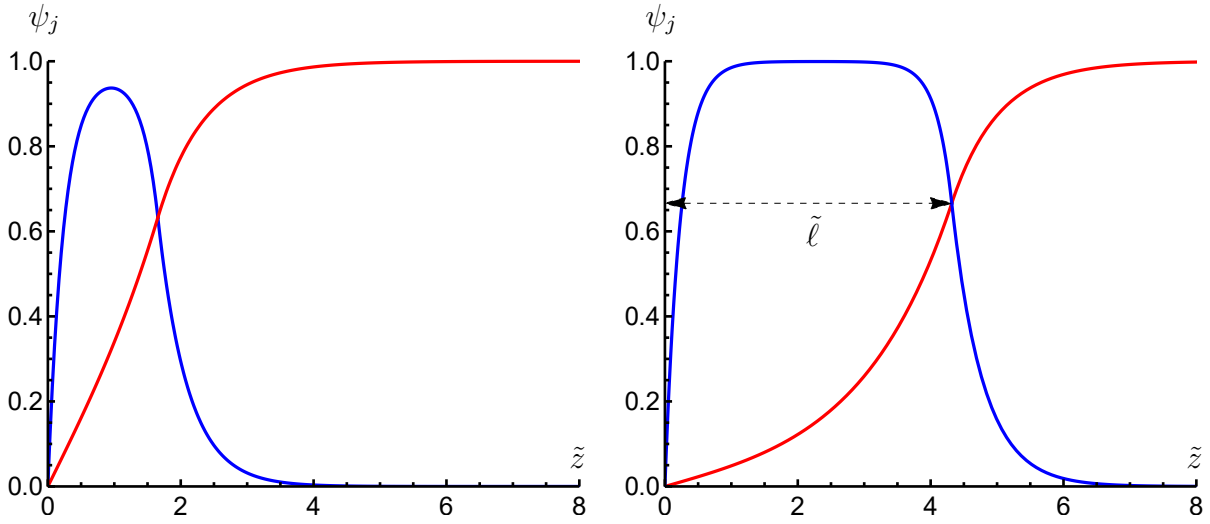

(a) $\epsilon = 0.95$ (b) $\epsilon = 0.999$

Figure 3.3: The reduced order parameter of the two condensate components as a function of $\tilde{z}$ at $\xi = 1/3$ and $K = 1.5$.

The thickness of the prewetting layer is determined by the condition

$$\psi_1(\tilde{\ell}) = \psi_2(\tilde{\ell}) \tag{3.11}$$

whose analytical solution is given by

$$\tilde{\ell} \approx \frac{1}{2\sqrt{\epsilon K - 1}} \ln\left(\frac{\sqrt{K-\epsilon} + \sqrt{2\epsilon}(1-\sqrt{\epsilon}) + \epsilon\sqrt{\epsilon K - 1}}{\sqrt{K-\epsilon} + \sqrt{2\epsilon}(1-\sqrt{\epsilon}) - \epsilon\sqrt{\epsilon K - 1}}\right). \tag{3.12}$$

Looking at Fig. 3.3, we see that the thickness of the prewetting layer increases as the chemical potential increases.

From Eq. (3.12) we see that the thickness of the prewetting layer depends on the relative interaction strength K and the chemical potential ratio ϵ, but does not depend on the specific value of ξ. It is worth noting that the denominator inside the logarithm in Eq. (3.12) does not vanish when the chemical potential gradually increases, which simply indicates that the thickness of the prewetting layer remains finite until the wetting transition occurs at $\epsilon = 1$. This also highlights an important point: the wetting transition in BECs occurs in an environment where the phase transition is first-order.

By expanding the logarithmic term in Eq. (3.12) for small $x = -\ln(1-\epsilon)$, we obtain

$$\tilde{\ell} \approx \frac{1}{2\sqrt{K-1}} \left[x - \ln\left(\frac{3K + \sqrt{2(K-1)} - 1}{4(K-1)}\right)\right]. \tag{3.13}$$

Clearly, the thickness of the prewetting layer varies linearly with x, which is consistent with the plot shown below.

Thus, both the theoretical results for the thickness of prewetting layer calculated using the GP and DPA models show that the thickness of the prewetting layer can be

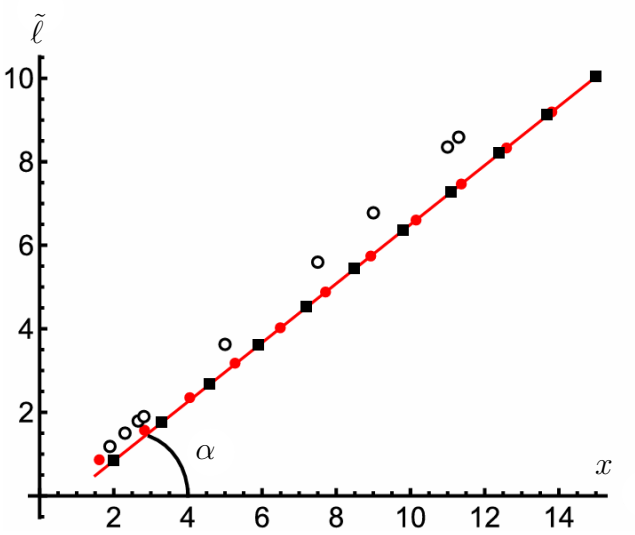

Figure 3.4: The thickness of prewetting layer as a function of chemical potential ratio in logarithm scale at $K = 1.5$. The solid line is plotted by solving numerical (3.11). The circles and squares simulate for (3.12) and (3.13), respectively. The open circles are results from numerical computation within GP theory.

represented as a linear function of x with a slope $a = \tan\alpha$, where α is the angle formed by the graph $\ell(x)$ and the x-axis (as shown in Figure 3.4). In DPA, the slope obtained from (3.13) is

$$a_{\rm DPA} = \frac{1}{2\sqrt{K-1}}. \tag{3.14}$$

This relation shows that the angle α decreases as the relative interaction strength K increases. In Table 3.1, we present the values for $a_{\rm DPA}$, $a_{\rm GP}$, and the corresponding relative error

$$\delta = \frac{|a_{\rm GP} - a_{\rm DPA}|}{a_{\rm GP}}. \tag{3.15}$$

The important observation here is that the relative error of DPA compared to the GP theory is less than 10%.

K	$a_{\rm DPA}$	$a_{\rm GP}$	δ (%)
1.1	0	0	0
1.3	0.913	0.916	0.36
1.5	0.707	0.756	6.53

Table 3.1: The slope a in GP and DPA models, with the corresponding relative error.

3.3.2 Thermodynamic contact angle

According to Young's law, the thermodynamic contact angle θ satisfies the mechanical equilibrium condition of a three-phase contact line,

$$\gamma_{\rm W1} = \gamma_{\rm W2} + \gamma_{12}\cos\theta. \tag{3.16}$$

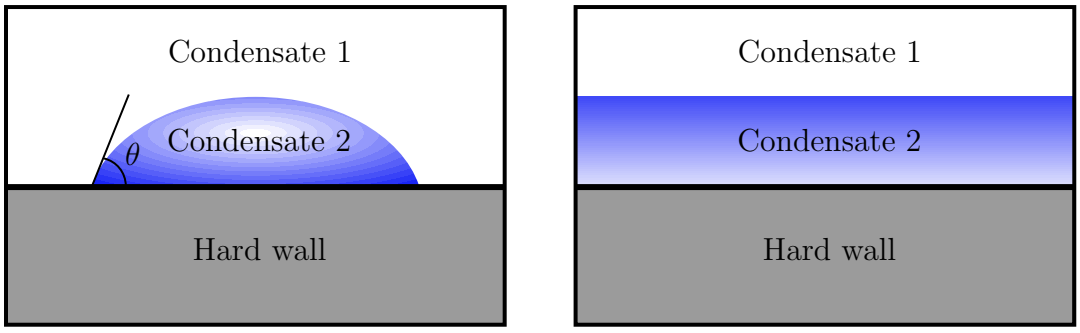

Figure 3.5: A two-component Bose–Einstein condensate mixture adsorbed on a hard wall in the prewetting phase (left), and in the wetting phase (right).

The tension at the interface between two condensates is the excess grand potential per unit area. Mathematically, it can be determined by the order parameter through the following relation:

$$\gamma_{12} = 4P\xi_1 \int_0^\infty d\tilde{z} \left[\left(\frac{d\psi_1}{d\tilde{z}} \right)^2 + \xi^2 \left(\frac{d\psi_2}{d\tilde{z}} \right)^2 \right]. \tag{3.17}$$

Substituting (3.2) and (3.3) into (3.17), we obtain

$$\gamma_{12} = P\left(M\xi_1 + N\bar{\xi}_2\right), \tag{3.18}$$

where M and N are constants depending on ϵ, K and ξ.

In DPA model, the surface tension of condensate j with respect to the wall is

$$\gamma_{\mathrm{W}j,\mathrm{pure}} = 2\sqrt{2}P_j\xi_j. \tag{3.19}$$

In the system with two condensates, we are currently considering the case where the condensate on the right is in the bulk, while the condensate on the left is adsorbed by a rigid wall. Therefore, the surface tension of condensate 1 is defined as the difference between the total free energy of the system and that of the large volume occupied by the pure phase 1 in the bulk, from the GP equation (3.1) we have:

In the condensate system we are considering, condensate 1 is on the right side of the interface, while condensate 2 is adsorbed by a hard wall. Therefore, the surface tension of condensate 1 at the wall is defined as the excess per unit area between the total grand potential of the system and the grand potential of the half-space filled with pure phase 1 in bulk-phase, from the GP system of equations (3.1) we have

$$\gamma_{\mathrm{W1}} = \gamma_{\mathrm{W1,pure}} + \gamma_{\mathrm{W2,pure}} - 2P_1\xi_1 \int_0^\infty K\psi_1^2\psi_2^2 d\tilde{z}. \tag{3.20}$$

Nearly the coexistence line ($\epsilon = 1$ in Fig. 3.2), the interfacial tension can be reduced

$$\gamma_{12} = 2\sqrt{2}P\left(\xi_1 \frac{\sqrt{\epsilon K - 1}}{\sqrt{2} + \sqrt{\epsilon K - 1}} + \bar{\xi}_2 \frac{\epsilon^{3/2}\left[K - \epsilon + \sqrt{2\epsilon(K-\epsilon)}\right]}{\left(\sqrt{2\epsilon} + \sqrt{K-\epsilon}\right)^2} \right). \tag{3.21}$$

In first order approximation of the $(1-\epsilon)$, (3.21) can be written as

$$\gamma_{12} \approx 2\sqrt{2}P\left(\xi_1 + \bar{\xi}_2\right) \frac{\sqrt{K-1}}{\sqrt{2} + \sqrt{K-1}} + F(K,\xi)(1-\epsilon), \tag{3.22}$$

where $F(K, \xi)$ is a function of K and ξ.

At the wetting phase ($\theta = 0$), the last term on the right-hand side of (3.20) will be zero. Combining (3.16), (3.19), (3.20), and (3.21), we determined the wetting phase boundary in the $(\xi, 1/K)$ plane, which has the equation

$$\sqrt{K-1} = \frac{1}{\sqrt{2}} \left(\frac{1}{\xi} - 1 \right). \tag{3.23}$$

Furthermore, we determined the contact angle θ that satisfies

$$\cos\theta = \frac{\gamma_{\mathrm{W1}} - \gamma_{\mathrm{W2,pure}}}{\gamma_{12}}. \tag{3.24}$$

Approach the coexistence line, the cosine of the contact angle is able to be expressed in terms of ξ and K:

$$\cos\theta \approx \left(\frac{1-\xi}{1+\xi} \right) \frac{\sqrt{2} + \sqrt{K-1}}{\sqrt{K-1}}. \tag{3.25}$$

From (3.25), we see that in the case of a weakly separated system:

$$\cos\theta \approx \left(\frac{1-\xi}{1+\xi} \right) \frac{\sqrt{2}}{\sqrt{K-1}}. \tag{3.26}$$

Conversely, in the case of a strongly separated system, the contact angle will not depend on the relative interaction strength K:

$$\cos\theta \approx \frac{1-\xi}{1+\xi}. \tag{3.27}$$

Equation (3.27) once again confirms that, when the relative interaction strength is sufficiently large, the contact angle depends only on the relative characteristic length. Moreover, (3.27) also shows that the contact angle is always non-zero when the relative interaction strength is sufficiently large. This indicates that the wetting phase transition does not occur for a very strongly separated system.

Chapter 4

Thermodynamic properties of dilute Bose gas at finite temperature

4.1 Thermodynamic properties of dilute Bose gas in the one-loop approximation

We start from the Lagrangian density of a homogeneous dilute Bose gas

$$\mathcal{L} = \Psi^* \left(-i\hbar \frac{\partial}{\partial t} - \frac{\hbar^2}{2m} \nabla^2 \right) \Psi - \mu |\Psi|^2 + \frac{g}{2} |\Psi|^4. \tag{4.1}$$

In the tree-level approximation, the expectation value $\Psi_0 = \sqrt{\mu/g}$ of the field operator corresponds to the spontaneously broken symmetry phase. The propagator within this approximation is

$$G_0(k) = \frac{1}{\hbar^2 \omega_n^2 + E_0^2(k)} \begin{pmatrix} \frac{\hbar^2 k^2}{2m} - \mu + g\Psi_0^2 & \hbar\omega_n \\ -\hbar\omega_n & \frac{\hbar^2 k^2}{2m} - \mu + 3g\Psi_0^2 \end{pmatrix}, \tag{4.2}$$

where $\omega_n = 2\pi n \hbar^{-1} \beta^{-1}$ $(n \in \mathbb{Z})$ is the Matsubara frequency for bosons at temperature T. The dispersion relation is determined through the components on the main diagonal of the propagator

$$E_0(k) = \sqrt{\frac{\hbar^2 k^2}{2m} \left(\frac{\hbar^2 k^2}{2m} + 2g\Psi_0^2 \right)}. \tag{4.3}$$

This dispersion relation shows that the energy spectrum of the elementary excitation is gapless, i.e., at $k = 0$ then $E_0 = 0$. This corresponds to the spontaneous breaking of the $U(1)$ symmetry and is consistent with the Goldstone theorem.

4.1.1 Condensate depletion và critical temperature

In the one-loop approximation, the CJT effective potential corresponding to the Lagrangian (4.1) takes the form

$$V_{\mathrm{CJT}} = -\mu\Psi_0^2 + \frac{g}{2}\Psi_0^4 + \frac{1}{2} \int_\beta \mathrm{tr} \left[\ln G^{-1}(k) \right], \tag{4.4}$$

where the propagator $G(k)$ within one-loop approximation is

$$G(k) = \frac{1}{\hbar^2\omega_n^2 + E(k)^2} \begin{pmatrix} \frac{\hbar^2 k^2}{2m} - \mu + g\Psi_0^2 & \hbar\omega_n \\ -\hbar\omega_n & \frac{\hbar^2 k^2}{2m} - \mu + 3g\Psi_0^2 \end{pmatrix}. \tag{4.5}$$

The corresponding dispersion relation is

$$E(k) = \sqrt{\left(\frac{\hbar^2 k^2}{2m} - \mu + g\Psi_0^2\right)\left(\frac{\hbar^2 k^2}{2m} - \mu + 3g\Psi_0^2\right)} = \sqrt{\frac{\hbar^2 k^2}{2m}\left(\frac{\hbar^2 k^2}{2m} + 2\mu\right)}. \tag{4.6}$$

In the limit of long wavelengths, it is easy to see that the energy spectrum of the elementary excitation is linearly proportional to the wave vector

$$E(k) \approx \hbar k\sqrt{\frac{\mu}{m}}, \tag{4.7}$$

which is consistent with the Nambu-Goldstone boson spectrum due to the spontaneous breaking of $U(1)$ symmetry.

To determine the last term on the right-hand side of (4.4), we apply the Matsubara summation method:

$$\frac{1}{\beta}\sum_{n=-\infty}^{+\infty} \ln\left[\hbar^2\omega_n^2 + E(k)^2\right] = E(k) + \frac{2}{\beta}\ln\left(1 - e^{-\beta E(k)}\right), \tag{4.8}$$

from which we obtain

$$V_{\mathrm{CJT}} = -\mu\Psi_0^2 + \frac{g}{2}\Psi_0^4 + \frac{1}{2}\int \frac{d^3\mathbf{k}}{(2\pi)^3}\left[E(k) + \frac{2}{\beta}\ln\left(1 - e^{-\beta E(k)}\right)\right]. \tag{4.9}$$

By minimizing the effective potential (4.9) with respect to Ψ_0, we obtain the gap equation within the one-loop approximation:

$$-\mu + g\rho_0 + \frac{g}{2}\int \frac{d^3\mathbf{k}}{(2\pi)^3}\left[2\left(\frac{\hbar^2 k^2}{2m} - \mu + 2g\Psi_0^2\right) - g\Psi_0^2\right]\frac{1}{E(k)}\left(1 + \frac{2}{e^{\beta E(k)} - 1}\right) = 0. \tag{4.10}$$

Substituting $\mu = g\rho$ into (4.10), we obtain the condensate density

$$\rho_0 = \frac{\mu}{g} - \int \frac{d^3\mathbf{k}}{(2\pi)^3}\left(\frac{\hbar^2 k^2}{m} + \mu\right)\frac{1}{E(k)}\left(\frac{1}{2} + \frac{1}{e^{\beta E(k)} - 1}\right). \tag{4.11}$$

The pressure is determined by

$$P = -V_{\mathrm{CJT}}|_{\min} = \frac{\mu^2}{2g} - \frac{1}{2}\int \frac{d^3\mathbf{k}}{(2\pi)^3}\left[E(k) + \frac{2}{\beta}\ln\left(1 - e^{-\beta E(k)}\right)\right]. \tag{4.12}$$

The total particle density is defined as the partial derivative of the pressure with respect to the chemical potential:

$$\rho = \frac{\partial P}{\partial \mu}. \tag{4.13}$$

Substituting (4.12) into (4.13), we obtain the total density

$$\rho = \frac{\mu}{g} - \int \frac{d^3\mathbf{k}}{(2\pi)^3} \frac{\hbar^2 k^2}{2m} \frac{1}{E(k)} \left(\frac{1}{2} + \frac{1}{e^{\beta E(k)} - 1} \right). \tag{4.14}$$

From (4.11) and (4.14), the condensate depletion within the one-loop approximation (also called the Popov approximation) is defined by

$$\frac{\rho_{\rm ex}}{\rho} \equiv \frac{\rho - \rho_0}{\rho} = \int \frac{d^3\mathbf{k}}{(2\pi)^3} \left(\frac{\hbar^2 k^2}{2m\rho} + g \right) \frac{1}{E(k)} \left(\frac{1}{2} + \frac{1}{e^{\beta E(k)} - 1} \right). \tag{4.15}$$

When the self-consistent condition is satisfied, the condensate depletion keeps the same form as Eq. (4.14) with the condensate density ρ_0 replaced by the total density ρ. Specifically, on the right-hand side of (4.14), we can take

$$E(k) = \sqrt{\frac{\hbar^2 k^2}{2m} \left(\frac{\hbar^2 k^2}{2m} + 2g\rho \right)}. \tag{4.16}$$

Setting $\kappa^2 = \dfrac{\hbar^2 k^2}{2m}$ and substituting (4.16) into (4.15), we obtain

$$\frac{\rho_{\rm ex}}{\rho} = \frac{(2m)^{3/2}}{\hbar^3 \rho} \int \frac{d^3\vec{\kappa}}{(2\pi)^3} \frac{\kappa^2 + g\rho}{\sqrt{\kappa^2(\kappa^2 + 2g\rho)}} \left(\frac{1}{2} + \frac{1}{e^{\beta\sqrt{\kappa^2(\kappa^2+2g\rho)}} - 1} \right) \tag{4.17}$$

The right-hand side of (4.17) is ultraviolet divergent. Using dimensional regularization, we have the integral

$$I_{m,n}(\mathcal{M}) = \int \frac{d^d\vec{\kappa}}{(2\pi)^d} \frac{\kappa^{2m-n}}{(\kappa^2 + \mathcal{M}^2)^{n/2}} = \frac{\Omega_d}{(2\pi)^d} \Lambda^{2\epsilon} \mathcal{M}^{d+2(m-n)} \frac{\Gamma(\frac{d-n}{2} + m)\Gamma(n - m - \frac{d}{2})}{2\Gamma(\frac{n}{2})}, \tag{4.18}$$

where $\Gamma(n) = \int_0^\infty x^{n-1} e^{-x} dx$ is the Gamma function, $\Omega_d = 2\pi^{d/2}/\Gamma(d/2)$ is the surface area of a unit d-dimensional sphere và Λ is the renormalization scale introduced to ensure that the expression has the correct physical dimension. Applying this result to $d = 3$ and using the condition $g\rho \ll k_{\rm B}T$ (or $\beta g\rho \ll 1$), we obtain

$$\frac{\rho_{\rm ex}}{\rho} = \frac{8}{3\sqrt{\pi}} \sqrt{\rho a_s^3} + \frac{\zeta(3/2)}{\rho \lambda_{\rm B}^3} + \frac{2\zeta(1/2) a_s}{\lambda_{\rm B}}, \tag{4.19}$$

where $\lambda_{\rm B}$ is the thermal de Broglie wavelength, given by

$$\lambda_{\rm B} = \sqrt{\frac{2\pi\hbar^2}{m k_{\rm B} T}}. \tag{4.20}$$

To determine the critical temperature, we impose the condition that the condensate fraction vanishes ($\rho_0 = 0$ and $\rho_{\rm ex} = \rho$) at the transition critical point. From Eq. (4.19), we obtain the expression for the critical temperature, including the first-order correction in a_s as follows:

$$T_{\rm c} = \frac{2\pi\hbar^2}{m k_{\rm B}} \left(\frac{\rho}{\zeta(3/2)} \right)^{2/3} \left(1 - \frac{4\zeta(1/2)}{3\zeta(3/2)^{1/3}} \rho^{1/3} a_s \right). \tag{4.21}$$

Thus, the relative shift of the critical temperature is linearly proportional to the s-wave scattering length according to

$$\frac{\Delta T_{\rm c}}{T_{\rm c}^{(0)}} = c\rho^{1/3}a_s, \tag{4.22}$$

where $c = -\dfrac{4\zeta(1/2)}{3\zeta(3/2)^{1/3}} \approx 1.413$. The result in Eq. (4.22) is in reasonably good agreement with Monte Carlo simulations ($c = 1.29 \pm 0.05$) and lattice simulations ($c = 1.32 \pm 0.02$). In addition, it is also close to the values obtained from the non-perturbative linear δ-expansion method in optimized perturbation theory ($c = 1.48$). The variational approach combined with asymptotic analysis based on Bogoliubov theory also yields a result consistent with ours ($c = 1.49$), however, that method leads to the conclusion that the transition is first order, which is inconsistent with the well-established fact that the Bose–Einstein condensation transition is second order.

4.1.2 Zero-point energy and thermodynamic properties of a Bose-condensed gas

Eq. (4.14) leads to the chemical potential

$$\mu = g\rho + g\int \frac{d^3\mathbf{k}}{(2\pi)^3}\frac{\hbar^2k^2}{2m}\frac{1}{E(k)}\left(\frac{1}{2} + \frac{1}{e^{\beta E(k)}-1}\right). \tag{4.23}$$

Substituting (4.16) into (4.23) and eliminating ultraviolet divergence through integral (4.18), we arrive, to leading order in the gas parameter ρa_s^3, at the following expression

$$\mu = g\rho\left(1 + \frac{32}{3\sqrt{\pi}}\sqrt{\rho a_s^3}\right) + \frac{4\pi\hbar^2\zeta(3/2)a_s}{m\lambda_{\rm B}^3}. \tag{4.24}$$

We now consider the pressure under the self-consistent condition. From Eq. (4.12), we have

$$\begin{aligned} P &= \frac{\mu^2}{2g} - \frac{1}{2}\int \frac{d^3\mathbf{k}}{(2\pi)^3}\sqrt{\kappa^2(\kappa^2+2\mu)} - \frac{1}{\beta}\int \frac{d^3\mathbf{k}}{(2\pi)^3}\ln\left(1 - e^{-\beta\sqrt{\kappa^2(\kappa^2+2\mu)}}\right) \\ &= \frac{\mu^2}{2g} + P_{\rm g}^{(0)} + P_{\rm g}^{(T)}. \end{aligned} \tag{4.25}$$

The second term on the right-hand of Eq. (4.25) represents the zero-point (vacuum) energy, which generates quantum fluctuations in the ground state:

$$\begin{aligned} \mathcal{E}_0 = -P_{\rm g}^{(0)} &= \frac{1}{2}\int \frac{d^3\mathbf{k}}{(2\pi)^3}\sqrt{\kappa^2(\kappa^2+2\mu)} = \frac{(2m)^{3/2}}{2\hbar^3}\int \frac{d^3\vec{\kappa}}{(2\pi)^3}\sqrt{\kappa^2(\kappa^2+2\mu)} \\ &= \frac{8m^{3/2}}{15\pi^2\hbar^3}\mu^{5/2}. \end{aligned} \tag{4.26}$$

With the dilute-gas condition and the vicinity of the condensation point taken into account, the last term on the right-hand side of Eq. (4.25) is approximated as

$$P_{\rm g}^{(T)} = \frac{2\pi\hbar^2}{m\lambda_{\rm B}^5}\left(\zeta(5/2) - \zeta(3/2)\frac{\mu}{k_{\rm B}T}\right). \tag{4.27}$$

Substituting Eqs. (4.26) and (4.27) into Eq. (4.25), we obtain the pressure satisfying the self-consistent condition, in the lowest-order approximation of the gas parameter, as follows:

$$P = \frac{g\rho^2}{2}\left(1 + \frac{64}{5\sqrt{\pi}}\sqrt{\rho a_s^3}\right) + \frac{2\pi\hbar^2\zeta(3/2)^2 a_s}{m\lambda_{\mathrm{B}}^6} + \frac{2\pi\hbar^2\zeta(5/2)}{m\lambda_{\mathrm{B}}^5}. \tag{4.28}$$

We now examine the physical meaning of the terms on the right-hand side of Eq. (4.28). The first term consists of two contributions: it is clear that the part $g\rho^2/2$ represents the bulk pressure, while the remaining part arises from quantum fluctuations at zero temperature (vacuum fluctuations). The next two terms describe the contributions of the interaction between atoms and thermal fluctuations to the pressure, in which the last term characterizes the pure thermal fluctuations, since it remains on the right-hand side of Eq. (4.28) even for an ideal Bose gas. This shows that the pressure of an ideal Bose gas in the condensed phase scales as $T^{5/2}$.

The energy density is determined from the pressure through the thermodynamic relation between these two quantities:

$$\mathcal{E} = -\left[\frac{\partial(\beta P)}{\partial\beta}\right]_{\beta\mu}. \tag{4.29}$$

Substituting (4.24) and (4.28) into (4.29), we obtain

$$\mathcal{E} = \frac{g\rho^2}{2}\left(1 + \frac{128}{15\sqrt{\pi}}\sqrt{\rho a_s^3}\right) - \frac{2\pi\hbar^2\zeta(3/2)\rho a_s}{m\lambda_{\mathrm{B}}^3} + \frac{4\pi\hbar^2\zeta(3/2)^2 a_s}{m\lambda_{\mathrm{B}}^6} + \frac{3\pi\hbar^2\zeta(5/2)}{m\lambda_{\mathrm{B}}^5}. \tag{4.30}$$

At finite temperature, the contributions of thermal fluctuations to the energy density are contained in the last three terms.

4.1.3 Thermodynamic properties of a dilute Bose gas in the normal phase

In the normal phase, the dispersion relation takes the form:

$$E(k) = \frac{\hbar^2 k^2}{2m} - \bar{\mu}, \tag{4.31}$$

where $\bar{\mu} = \mu - 2g\rho$ denotes the effective chemical potential, which reduces to the chemical potential of an ideal Bose gas in the normal phase. The corresponding propagator is given by

$$G(k) = \frac{1}{\hbar^2\omega_n^2 + E(k)^2}\begin{pmatrix} \dfrac{\hbar^2 k^2}{2m} - \bar{\mu} & \hbar\omega_n \\ -\hbar\omega_n & \dfrac{\hbar^2 k^2}{2m} - \bar{\mu} \end{pmatrix} \tag{4.32}$$

The ultraviolet divergence in the zero-point energy can be eliminated through the introduction of a counterterm, ensuring that it does not contribute to the pressure. The self-consistent pressure is then given

$$P = g\rho^2 + \frac{2\pi\hbar^2}{m\lambda_{\mathrm{B}}^5}\,\mathrm{Li}_{5/2}[e^{\beta(\mu-2g\rho)}]. \tag{4.33}$$

By substituting (4.33) into (4.13), we obtain the total particle density

$$\rho = \frac{\mathrm{Li}_{5/2}[e^{\beta(\mu-2g\rho)}]}{\lambda_{\mathrm{B}}^3}. \tag{4.34}$$

Inverting Eq. (4.34) yields the chemical potential

$$\mu = 2g\rho + k_{\mathrm{B}}T \ln\left[\mathrm{Li}^{-1}_{3/2}(\rho\lambda^3_{\mathrm{B}})\right]. \tag{4.35}$$

Combining Eqs. (4.24) and (4.35), we obtain the temperature dependence of the chemical potential near the critical point as follows:

$$\mu = \begin{cases} g\rho\left(1 + \dfrac{32}{3\sqrt{\pi}}\sqrt{\rho a_s^3}\right) + \dfrac{4\pi\hbar^2\zeta(3/2)a_s}{m\lambda^3_{\mathrm{B}}}, & T \le T_{\mathrm{c}}; \\ 2g\rho + k_{\mathrm{B}}T \ln\left[\mathrm{Li}^{-1}_{3/2}(\rho\lambda^3_{\mathrm{B}})\right], & T \ge T_{\mathrm{c}}. \end{cases} \tag{4.36}$$

The temperature dependence of the chemical potential given in Eq. (4.36) is shown by the black curve in Fig. 4.1. As can be seen, the chemical potential varies continuously across the condensation transition. Initially, in the condensed phase, the chemical potential increases with temperature from the value $g\rho$ to its maximum value $2g\rho$ at the critical point, after which it decreases as the temperature continues to rise. In Fig. 4.1, the red curve represents the temperature dependence of the chemical potential for an ideal Bose gas, while the circular and triangular markers indicate the experimental data reported by Mordini et al. (2020).

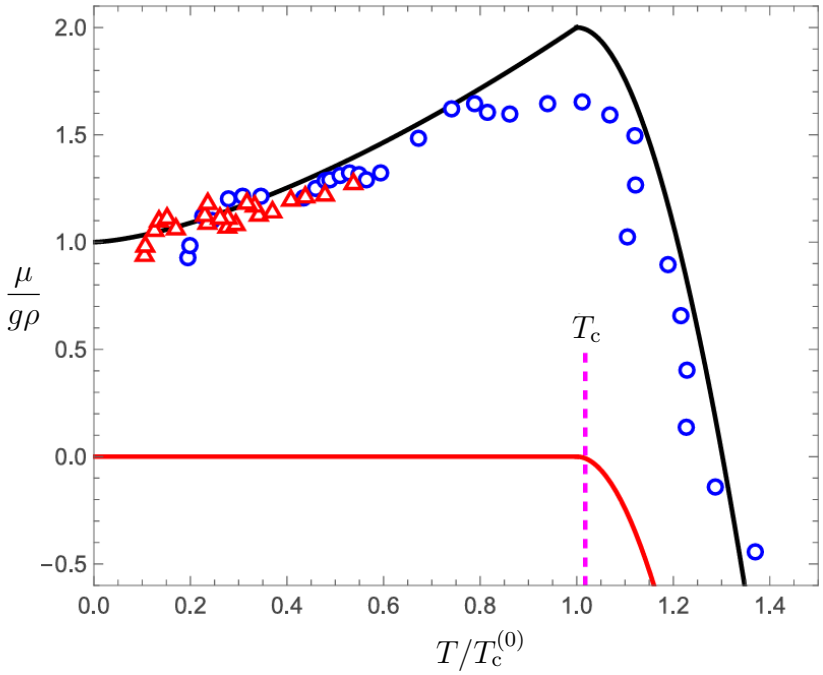

Figure 4.1: The evolution of the chemical potential of the sodium-23 (^{23}Na) gas versus the reduced temperature.

The experimental results show good agreement with our theoretical predictions. Another important feature that can be observed from Fig. 4.1 is the experimental confirmation of the non-monotonic behavior of the chemical potential in the vicinity of the transition point.

In a manner analogous to how we determined the chemical potential outside the condensed phase, the energy density at temperatures $T > T_{\mathrm{c}}$ is found to be of the form:

$$\mathcal{E} = g\rho^2 - \frac{2\pi\hbar^2}{m\lambda^5_{\mathrm{B}}}\,\mathrm{Li}_{5/2}[e^{\beta(\mu-2g\rho)}]. \tag{4.37}$$

4.2 Thermodynamic properties of dilute Bose gas in the two-loop approximation

4.2.1 The equations of state in condensed phase

We start from the CJT effective potential density within the Hartree–Fock approximation

$$V_{\rm CJT} = -\mu\Psi_0^2 + \frac{g}{2}\Psi_0^4 + \frac{1}{2}\int_\beta \mathrm{tr}\left[\ln G^{-1}(k) + G_0^{-1}(k)G(k) - \mathbb{1}\right] + \frac{3g}{8}\left(P_{11}^2 + P_{22}^2\right) + \frac{g}{4}P_{11}P_{22}. \tag{4.38}$$

From the CJT effective potential density (4.38), we derive:

- Gap equation:

$$-\mu + g\Psi_0^2 + \Pi_1 = 0. \tag{4.39}$$

- Schwinger–Dyson (SD) equation:

$$G^{-1}(k) = G_0^{-1}(k) + \Pi, \tag{4.40}$$

where $\Pi = \begin{pmatrix} \Pi_1 & 0 \\ 0 & \Pi_2 \end{pmatrix}$ is self-energies matrix, with $\Pi_1 = \frac{3g}{2}P_{11} + \frac{g}{2}P_{22}$ and $\Pi_2 = \frac{g}{2}P_{11} + \frac{3g}{2}P_{22}$.

The propagator within HF approximation takes the form:

$$G(k) = \frac{1}{\hbar^2\omega_n^2 + E_{\rm (HF)}^2(k)} \begin{pmatrix} \frac{\hbar^2k^2}{2m} - \mu + g\Psi_0^2 + \Pi_2 & -\hbar\omega_n \\ \hbar\omega_n & \frac{\hbar^2k^2}{2m} - \mu + 3g\Psi_0^2 + \Pi_1 \end{pmatrix}. \tag{4.41}$$

This propagator leads to the corresponding dispersion relation

$$E_{\rm (HF)}(k) = \sqrt{\left(\frac{\hbar^2k^2}{2m} - \mu + 3g\Psi_0^2 + \Pi_1\right)\left(\frac{\hbar^2k^2}{2m} - \mu + g\Psi_0^2 + \Pi_2\right)}. \tag{4.42}$$

Eq. (4.42) shows the appearance of an energy gap in the elementary excitation spectrum, which means that the Goldstone theorem is violated in the HF approximation.

To address this problem, we make use of the IHF approximation. In this scheme, the effective potential density is augmented by an additional correction term so that the equations of motion remain unchanged in form, and this yields

$$\tilde{V}_{\rm CJT} = -\mu\Psi_0^2 + \frac{g}{2}\Psi_0^4 + \frac{1}{2}\int_\beta \mathrm{tr}\left[\ln G_{\rm (IHF)}^{-1}(k) + G_0^{-1}(k)G_{\rm (IHF)}(k) - \mathbb{1}\right] + \frac{g}{8}\left(P_{11}^2 + P_{22}^2\right) + \frac{3g}{4}P_{11}P_{22}. \tag{4.43}$$

From the CJT effective potential density (4.43) within IHF approximation, we derive:

- Gap equation:

$$-\mu + g\Psi_0^2 + \Sigma_2 = 0, \tag{4.44}$$

- SD equation:

$$G_{\rm (IHF)}^{-1} = G_0^{-1} + \Sigma, \tag{4.45}$$

where $\Sigma = \begin{pmatrix} \Sigma_1 & 0 \\ 0 & \Sigma_2 \end{pmatrix}$ is self-energies matrix within IHF approximation, with $\Sigma_1 = \frac{g}{2}P_{11} + \frac{3g}{2}P_{22}$ and $\Sigma_2 = \frac{3g}{2}P_{11} + \frac{g}{2}P_{22}$.

The propagator within IHF approximation takes the form:

$$G_{(\mathrm{IHF})}(k) = \frac{1}{\hbar^2\omega_n^2 + E(k)^2} \begin{pmatrix} \frac{\hbar^2k^2}{2m} & \hbar\omega_n \\ -\hbar\omega_n & \frac{\hbar^2k^2}{2m} + M \end{pmatrix}, \tag{4.46}$$

where M denotes the effective mass, and the SD equation yields

$$M = -\mu + 3g\Psi_0^2 + \Sigma_1. \tag{4.47}$$

It can be seen that the elementary excitation spectrum corresponds to the propagator (4.46) within IHF approximation

$$E(k) = \sqrt{\frac{\hbar^2k^2}{2m}\left(\frac{\hbar^2k^2}{2m} + M\right)} \to \hbar k\sqrt{\frac{M}{2m}} \text{ khi } k \to 0. \tag{4.48}$$

Hence, the problem of the energy gap appearing in the excitation spectrum is remedied within the IHF approximation.

The chemical potential μ is defined as the first derivative of the pressure P with respect to the total particle density ρ:

$$\mu = \frac{\partial P}{\partial \rho} = -\frac{\partial V_{\mathrm{CJT}}|_{\min}}{\partial \rho}, \tag{4.49}$$

inserting

$$\begin{aligned} P = -\tilde{V}_{\mathrm{CJT}}\Big|_{\min} &= \mu\Psi_0^2 - \frac{g}{2}\Psi_0^4 - \frac{1}{2}\int_\beta \mathrm{tr}\left[\ln G^{-1}_{(\mathrm{IHF})}(k)\right] - \frac{1}{2}\left(3g\Psi_0^2 - \mu - M^2\right)P_{11} \\ &- \frac{1}{2}\left(g\Psi_0^2 - \mu\right)P_{22} - \frac{g}{8}\left(P_{11}^2 + P_{22}^2\right) - \frac{3g}{4}P_{11}P_{22}, \end{aligned} \tag{4.50}$$

we obtain the chemical potential within two-loop approximation:

$$\mu = g\rho + gP_{11}. \tag{4.51}$$

Combining Eqs. (4.51), (4.44), and (4.47), we obtain the gap equation and the SD equation for the effective mass:

$$0 = -1 + \frac{\rho_0}{\rho} + \frac{1}{2\rho}(P_{11} + P_{22}), \tag{4.52a}$$

$$\mathcal{M} = -1 + \frac{3\rho_0}{\rho} - \frac{1}{2\rho}(P_{11} - 3P_{22}), \tag{4.52b}$$

where $\mathcal{M} = M/(g\rho)$ is the dimensionless effective mass..

4.2.2 The condensate depletion at near-zero temperatures

To determine the momentum integrals P_{11} and P_{22}, the Matsubara summation formula must be employed

$$\sum_{n=-\infty}^{\infty} \frac{1}{\hbar^2\omega_n^2 + E(k)^2} = \frac{\beta}{2E(k)} \left(1 + \frac{2}{e^{\beta E(k)} - 1}\right). \tag{4.53}$$

At near-zero temperatures, the momentum integrals have the following analytic expressions:

$$P_{11} = \frac{(2m)^{3/2} M^{3/2}}{6\pi^2\hbar^3} + \frac{(2m)^{3/2}\pi^2}{30\hbar^3 M^{5/2}} (k_{\mathrm{B}}T)^4, \tag{4.54a}$$

$$P_{22} = -\frac{(2m)^{3/2} M^{3/2}}{12\pi^2\hbar^3} + \frac{(2m)^{3/2}}{12\hbar^3 M^{1/2}} (k_{\mathrm{B}}T)^2. \tag{4.54b}$$

Substituting the momentum integrals in Eq. (4.54) into the gap equation (4.52a) and the SD equation (4.52b), we obtain the system of equations that describes the relation between the condensate fraction ρ_0/ρ and the dimensionless effective mass $\mathcal{M}$ at temperatures $T \gtrsim 0$ as follows:

$$0 = -1 + \frac{\rho_0}{\rho} + \frac{2\sqrt{2}}{3\sqrt{\pi}} \mathcal{M}^{3/2} \sqrt{\rho a_s^3} + \frac{(m k_{\mathrm{B}} T)^2}{12\sqrt{2\pi}\hbar^4 \rho^{3/2} a_s^{1/2} \mathcal{M}^{1/2}} + \frac{(m k_{\mathrm{B}} T)^4}{480\sqrt{2\pi}\hbar^8 \rho^{7/2} a_s^{5/2} \mathcal{M}^{5/2}}, \tag{4.55a}$$

$$\mathcal{M} = -1 + \frac{3\rho_0}{\rho} - \frac{10\sqrt{2}}{3\sqrt{\pi}} \mathcal{M}^{3/2} \sqrt{\rho a_s^3} + \frac{(m k_{\mathrm{B}} T)^2}{4\sqrt{2\pi}\hbar^4 \rho^{3/2} a_s^{1/2} \mathcal{M}^{1/2}} - \frac{(m k_{\mathrm{B}} T)^4}{480\sqrt{2\pi}\hbar^8 \rho^{7/2} a_s^{5/2} \mathcal{M}^{5/2}}. \tag{4.55b}$$

Solving the above system of equations, we obtain an approximate expression for the condensate depletion of a dilute Bose gas near-zero temperature:

$$\frac{\rho_{\mathrm{ex}}}{\rho} = 1 - \frac{\rho_0}{\rho} = \frac{8}{3\sqrt{\pi}} \sqrt{\rho a_s^3} + \frac{2(m k_{\mathrm{B}} T)^2}{9\pi\hbar^4 \rho} a_s + \frac{(m k_{\mathrm{B}} T)^4}{9\pi^{3/2}\hbar^8 \rho^{5/2}} a_s^{1/2}. \tag{4.56}$$

It can be seen that the right-hand side of Eq. (4.56) consists of two contributions: (i) a term characterizing the effect of pure quantum fluctuations, represented by the first term; and (ii) a term characterizing the influence of near-zero temperature effects, represented by the last two terms.

Our result differs from that obtained for an ideal homogeneous Bose gas, in which the condensate depletion scales as $T^{3/2}$. This discrepancy arises because the phonon part of the spectrum dominates most of the thermodynamic properties. This implies that introducing even a small interaction between particles can significantly modify the properties of a Bose gas at low temperatures.

In Fig. 4.2, the black curve represents the Bogoliubov theory, the blue curve shows our result in Eq. (4.56) at the temperature $T = 3.5\,\mathrm{nK}$, and the open circles are the experimental data of Lopes et al., with the shaded error band shown as the dark yellow curve. It can be seen that our theoretical prediction agrees reasonably well with the experimental measurements.

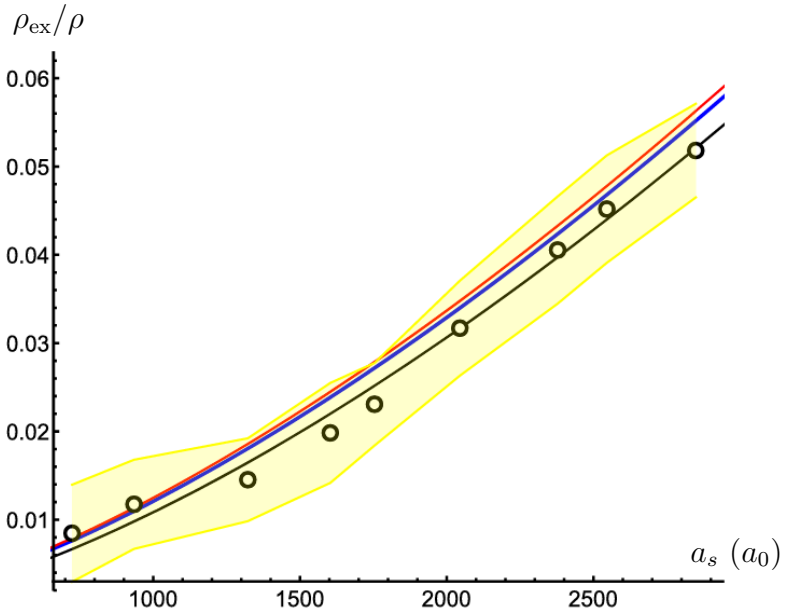

Figure 4.2: The condensate depletion of a homogeneous repulsive weakly interacting Bose gas as a function of the scattering length a_s at temperature $T = 3.5\,\mathrm{nK}$.

4.2.3 The condensate depletion near the critical temperature

Near the critical temperature, the momentum integrals take the following analytic forms:

$$P_{11} = \frac{(2m)^{3/2}M^{3/2}}{6\pi^2\hbar^3} + \left(\frac{mk_{\rm B}T}{2\pi\hbar^2}\right)^{3/2}\left(\zeta(3/2) - \frac{1}{2}\zeta(1/2)\frac{M}{k_{\rm B}T}\right), \tag{4.57a}$$

$$P_{22} = -\frac{(2m)^{3/2}M^{3/2}}{12\pi^2\hbar^3} + \left(\frac{mk_{\rm B}T}{2\pi\hbar^2}\right)^{3/2}\left(\zeta(3/2) + \frac{3}{2}\zeta(1/2)\frac{M}{k_{\rm B}T}\right). \tag{4.57b}$$

Substituting the momentum integrals in (4.57) into the gap equation (4.52a) and the SD equation (4.52b), we obtain the following system of equations that describes the relation between the condensate fraction ρ_0/ρ and the dimensionless effective mass $\mathcal{M}$ at temperatures $T \lesssim T_{\rm c}$:

$$0 = -1 + \frac{\rho_0}{\rho} + \frac{2\sqrt{2\rho a_s^3}}{3\pi}\mathcal{M}^{3/2} + t^{3/2}\left(1 + \frac{\zeta(1/2)\rho^{1/3}a_s}{\zeta(3/2)^{1/3}}\frac{\mathcal{M}}{t}\right), \tag{4.58a}$$

$$\mathcal{M} = -1 + \frac{3\rho_0}{\rho} - \frac{10\sqrt{2\rho a_s^3}}{3\pi}\mathcal{M}^{3/2} + t^{3/2}\left(1 + \frac{5\zeta(1/2)\rho^{1/3}a_s}{\zeta(3/2)^{1/3}}\frac{\mathcal{M}}{t}\right), \tag{4.58b}$$

where $t = T/T_{\rm c}^{(0)}$ is the ratio between the temperature and the ideal-gas critical temperature $T_{\rm c}^{(0)}$. Solving the above system of equations, we obtain

$$\sqrt{\mathcal{M}} \approx \sqrt{2} - \frac{16\sqrt{2}}{3\sqrt{\pi}}\sqrt{\rho a_s^3} - \frac{t^{3/2}}{\sqrt{2}} + \frac{\sqrt{2}\zeta(1/2)\rho^{1/3}a_s}{\zeta(3/2)^{1/3}}\sqrt{t}, \tag{4.59a}$$

$$\frac{\rho_0}{\rho} \approx 1 - \frac{8}{3\sqrt{\pi}}\sqrt{\rho a_s^3} - \left(1 - \frac{4}{\sqrt{\pi}}\sqrt{\rho a_s^3}\right)t^{3/2} - \frac{2\zeta(1/2)\rho^{1/3}a_s}{\zeta(3/2)^{1/3}}\sqrt{t}. \tag{4.59b}$$

Thus, the condensate depletion of a dilute Bose gas at temperatures T close to the critical

temperature is

$$\frac{\rho_{\rm ex}}{\rho} = \frac{8}{3\sqrt{\pi}}\sqrt{\rho a_s^3} + \left(1 - \frac{4}{\sqrt{\pi}}\sqrt{\rho a_s^3}\right)\left(\frac{T}{T_{\rm c}^{(0)}}\right)^{3/2} + \frac{2\zeta(1/2)\rho^{1/3}a_s}{\zeta(3/2)^{1/3}}\sqrt{\frac{T}{T_{\rm c}^{(0)}}}. \tag{4.60}$$

At the critical point ($T = T_{\rm c}$), the condensate fraction vanishes. This condition allows us to determine the critical temperature within the two-loop approximation

$$T_{\rm c} = \frac{2\pi\hbar^2}{mk_{\rm B}}\left(\frac{\rho}{\zeta(3/2)}\right)^{2/3}\left(1 - \frac{4\zeta(1/2)}{3\zeta(3/2)^{1/3}}\rho^{1/3}a_s + \frac{8}{9\sqrt{\pi}}\sqrt{\rho a_s^3}\right). \tag{4.61}$$

4.2.4 Thermodynamic functions

Because the thermodynamic functions of a Bose gas differ inside and outside the condensate phase, we examine the two distinct temperature regions, which are separated by the critical temperature.

Substituting (4.50) into (4.13), we express the particle density of the gas within the IHF approximation, in terms of the order parameter and the momentum integrals

$$\rho = \Psi_0^2 + \frac{g}{2}\left(P_{11} + P_{22}\right). \tag{4.62}$$

Substituting (4.62) into (4.50), we obtain

$$P = \frac{g\rho^2}{2} + g\rho P_{11} + \frac{g}{2}P_{11}^2 - \frac{1}{2}\int_\beta {\rm tr}\left[\ln G^{-1}_{\rm (IHF)}(k)\right] \tag{4.63}$$

$$= \frac{g\rho^2}{2}\left(1 + \frac{64}{5\sqrt{\pi}}\sqrt{\rho a_s^3}\right) + \frac{4\pi\hbar^2\zeta(3/2)\rho a_s}{m\lambda_{\rm B}^3} + \frac{2\pi\hbar^2\zeta(3/2)^2 a_s}{m\lambda_{\rm B}^6} + \frac{2\pi\hbar^2\zeta(5/2)}{m\lambda_{\rm B}^5}. \tag{4.64}$$

We see that the first term on the right-hand side of (4.64) is exactly the bulk pressure $P_0 = g\rho^2/2$, the next terms characterize the effects of quantum and thermal fluctuations on the pressure, in which the second term represents the contribution from pure quantum fluctuations.

By inserting (4.63) into (4.29), we obtain the energy density

$$\mathcal{E} = \frac{g\rho^2}{2}\left(1 + \frac{128}{15\sqrt{\pi}}\sqrt{\rho a_s^3}\right) + \frac{4\pi\hbar^2\zeta(3/2)\rho a_s}{m\lambda_{\rm B}^3} + \frac{2\pi\hbar^2\zeta(3/2)^2 a_s}{m\lambda_{\rm B}^6} + \frac{3\pi\hbar^2\zeta(5/2)}{m\lambda_{\rm B}^5}. \tag{4.65}$$

In the normal phase, at temperatures $T > T_{\rm c}$, the condensate density vanishes. In this phase, the dispersion relation (4.48) is modified into the form

$$E(k) = \frac{\hbar^2 k^2}{2m} - \bar{\mu}, \tag{4.66}$$

where $\bar{\mu} = \mu - \Sigma_1$ is the effective chemical potential.

The temperature-independent contributions in the momentum integrals come from quantum fluctuations. The ultraviolet divergence that appears here is removed by introducing a counterterm such that these terms do not contribute to the final result. The temperature-dependent contributions in the momentum integrals are the Bose integrals

The temperature-independent terms in the momentum integrals are ultraviolet divergent. This problem is resolved by introducing counterterms such that they do not contribute to the final results. The temperature-dependent terms in the momentum integrals take the form of Bose integrals,

$$P_{11} = P_{22} = \frac{4}{\sqrt{\pi}\lambda_{\rm B}^3}\,{\rm Li}_{3/2}(\bar{z}), \tag{4.67}$$

where $\bar{z} = e^{\beta\bar{\mu}}$ is the fugacity of the Bose gas. Because the condensate vanishes, the classical and zero-point contributions do not enter the result, and thus we obtain

$$\frac{1}{2}\int_{\beta} \mathrm{tr}\left[\ln G^{-1}(k)\right] = -\frac{2\pi\hbar^2}{m\lambda_{\mathrm{B}}^5}\,\mathrm{Li}_{5/2}(\bar{z}). \tag{4.68}$$

The pressure in the normal phase is easily derived as

$$P = gP_{11}^2 - \frac{1}{2}\int_{\beta} \mathrm{tr}\left[\ln G^{-1}(k)\right]. \tag{4.69}$$

Near the critical point, we can approximate $\bar{\mu} = \mu$ in the internal energy. In this case, Eqs. (4.67) and (4.68) allow us to rewrite the pressure (4.69) in the form

$$P = \frac{2\pi\hbar^2}{m\lambda_{\mathrm{B}}^5}\,\mathrm{Li}_{5/2}(\bar{z}) + \frac{64\pi\hbar^2 a_s}{m\lambda_{\mathrm{B}}^6}\,\mathrm{Li}_{3/2}^2(\bar{z}). \tag{4.70}$$

From (4.70), we derive total particle density

$$\rho = \frac{64a_s}{\pi\lambda_{\mathrm{B}}^4}\,\mathrm{Li}_{1/2}(\bar{z})\,\mathrm{Li}_{3/2}(\bar{z}) + \frac{1}{\lambda_{\mathrm{B}}^3}\,\mathrm{Li}_{3/2}(\bar{z}). \tag{4.71}$$

Solving the above equation, we obtain the expression for the polylogarithm function

$$\mathrm{Li}_{3/2}(\bar{z}) = \rho\lambda_{\mathrm{B}}^3\left[1 + \Lambda\left(-1 - \frac{\pi\ln\bar{z}}{64\rho a_s\lambda_{\mathrm{B}}^2}\right)\right], \tag{4.72}$$

where $\Lambda(x)$ is the Lambert function. For a dilute Bose gas at finite temperature, single-particle excitations dominate, which is equivalent to the condition that the thermal de Broglie wavelength is much smaller than the characteristic length scale, $\rho a_s\lambda_{\mathrm{B}}^2 \ll 1$. Therefore, to lowest order, the effective chemical potential can be inferred from (4.72) as follows

$$\bar{\mu} = k_{\mathrm{B}}T\ln\left[\mathrm{Li}_{3/2}^{-1}(\rho\lambda_{\mathrm{B}}^3)\right]. \tag{4.73}$$

The above equation is equivalent to

$$\mathrm{Li}_{3/2}(\bar{z}) = \rho\lambda_{\mathrm{B}}^3. \tag{4.74}$$

SUsing the derivative formula for the polylogarithm function applied to (4.74):

$$\frac{d\,\mathrm{Li}_n(\bar{z})}{d\bar{z}} = \frac{1}{\bar{z}}\,\mathrm{Li}_{n-1}(\bar{z}), \tag{4.75}$$

we can derive that

$$\mathrm{Li}_{5/2}(\bar{z}) = \frac{\lambda_{\mathrm{B}}^3 P}{k_{\mathrm{B}}T}, \tag{4.76}$$

where $P = \rho(\bar{\mu} + C)$, with C being a constant ensuring the continuity of the pressure P at the critical point. Equations (4.74) and (4.76) are in complete agreement with the equations of state of the ideal Bose gas, in which the effective chemical potential of the weakly interacting dilute Bose gas plays the role of the chemical potential of the ideal Bose gas.

Conclusion and outlook

1 Main results

In this doctoral thesis, we have obtained several important results that contribute to the understanding of the properties of both single-component and two-component Bose–Einstein condensate (BEC) systems. The main outcomes can be summarized as follows:

1. For the two-component dilute Bose gas: The properties of the prewetting phase are thoroughly investigated using the double parabola approximation (DPA) within the Gross–Pitaevskii (GP) theory. Our study shows that, in the prewetting phase, the thickness of the wetting layer increases linearly with the logarithm of the ratio of the chemical potentials as the system approaches the fully wetting phase. During this process, the contact angle decreases from a finite value (partial wetting) to zero (complete wetting). These findings will contribute to the design of experiments aimed at observing the wetting phase transition in BECs.

2. For the single-component dilute Bose gas:

- Our study shows that the Cornwall–Jackiw–Tomboulis (CJT) effective action framework describes very well the thermodynamic properties of dilute Bose gases not only at zero temperature but also at finite temperature. The relative shift of the critical temperature due to interparticle interactions obtained in this work agrees well with the corresponding results from numerical Monte Carlo simulations. The results obtained within the one-loop and two-loop approximations are also found to be in good agreement with each other.

- The use of the CJT effective action in the improved Hartree–Fock (IHF) approximation yields very good results for the thermodynamic properties of dilute Bose gases, especially the continuous and non-monotonic behavior of the chemical potential near the phase-transition temperature. This resolves the limitation of the standard Hartree–Fock theory, which predicts an unphysical discontinuity in the chemical potential at the transition point.

2 Recommendations for future research

The investigation of the wetting transition presented in this dissertation is carried out within the mean-field GP framework. This means that condensate depletion due to quantum fluctuations and thermal excitations has not been included. Such effects may lead to significant deviations from experimental observations when the system is not sufficiently cold, specifically when the temperature is only moderately below the critical temperature. In addition, the hard-wall boundary condition is an idealized model, and in current experiments it is generally not feasible to construct perfectly rigid boundaries of this type.

Building upon the results obtained in this thesis, we propose several potential directions for future research:

- At zero temperature: explore alternative boundary conditions to replace the ideal hard wall, with the aim of experimentally observing the wetting phenomenon in BEC systems.

- At finite temperature: assess the effect of temperature on the surface energy, and consequently examine its impact on the wetting transition in BECs.

List of papers related to the thesis

1. N. V. Thu and P. D. Thanh. Phenomenological analogy between Gross–Pitaevskii theory for Bose–Einstein condensate and Newton equation for classical mechanics. *VNU Journal of Science: Mathematics–Physics*, 40(2):100–105, 2024.

2. N. V. Thu and P. D. Thanh. Effect of nonzero temperature to non-condensed fraction of a homogeneous dilute weakly interacting Bose gas. *Physics Letters A*, 523:129787, 2024.

3. P. D. Thanh and N. V. Thu. Static properties of prewetting phase in binary mixtures of Bose–Einstein condensates. *International Journal of Theoretical Physics*, 63(12):315, 2024.

4. P. D. Thanh, T. K. Vi and N. V. Thu. Phenomenological analogy between Gross–Pitaevskii theory for Bose–Einstein condensate mixtures in infinite space and classical mechanics. *HNUE Journal of Science: Natural Science*, 70(1): 25–35, 2025.

5. N. V. Thu, P. D. Thanh and L. T. Thuy. Transition temperature and thermodynamic properties of homogeneous weakly interacting Bose gas in self-consistent Popov approximation. *Physica B: Condensed Matter*, 713:417356, 2025.

6. P. D. Thanh and D. T. Hai. The interface position of a Bose–Einstein condensate mixture restricted by a hard wall in double-parabola approximation. *Dalat University Journal of Science: Natural Sciences and Technology*, 15(3S):33–43, 2025.

7. P. D. Thanh and N. V. Thu. The thermodynamic contact angle in the prewetting phase of a binary Bose–Einstein condensate mixture. *HNUE Journal of Science: Natural Science*, 70(3): 35–46, 2025.

8. N. V. Thu and P. D. Thanh. Thermodynamic properties of repulsive interacting Bose gas at sufficiently temperature. *International Journal of Modern Physics B*, 2026.